The Astrophysical Journal, 826:82 (6pp), 2016 July 20 doi:10.3847/0004-637X/826/1/82

FAST RADIO BURSTS AND THEIR GAMMA-RAY OR RADIO AFTERGLOWS AS KERR–NEWMAN BLACK HOLE BINARIES

Tong Liu[1,2], Gustavo E. Romero[3,4], Mo-Lin Liu[5], and Ang Li[1,2]
[1] Department of Astronomy, Xiamen University, Xiamen, Fujian 361005, China; tongliu@xmu.edu.cn, liang@xmu.edu.cn
[2] Department of Physics and Astronomy, University of Nevada, Las Vegas, NV 89154, USA
[3] Instituto Argentino de Radioastronomía (IAR, CCT La Plata, CONICET), C.C.5, 1894 Villa Elisa, Buenos Aires, Argentina; romero@iar.unlp.edu.ar
[4] Facultad de Ciencias Astronómicas y Geofísicas, Universidad Nacional de La Plata, Paseo del Bosque s/n, 1900 La Plata, Argentina
[5] College of Physics and Electronic Engineering, Xinyang Normal University, Xinyang, Henan 464000, China; mlliu@xynu.edu.cn
Received 2016 February 28; revised 2016 May 10; accepted 2016 May 16; published 2016 July 25

ABSTRACT

Fast radio bursts (FRBs) are radio transients lasting only about a few milliseconds. They seem to occur at cosmological distances. We propose that these events can originate in the collapse of the magnetospheres of Kerr–Newman black holes (KNBHs). We show that the closed orbits of charged particles in the magnetospheres of these objects are unstable. After examining the dependencies on the specific charge of the particle and the spin and charge of the KNBH, we conclude that the resulting timescale and radiation mechanism fit well with extant observations of FRBs. Furthermore, we argue that the merger of a KNBH binary is a plausible central engine for the potential gamma-ray or radio afterglow following certain FRBs and can also account for gravitational wave (GW) events like GW 150914. Our model leads to predictions that can be tested by combined multi-wavelength electromagnetic and GW observations.

Key words: binaries: general – black hole physics – gamma-ray burst: general – gravitational waves

1. INTRODUCTION

Fast radio bursts (FRBs) are transient astrophysical sources with radio pulses lasting only about a few milliseconds and a total energy release of about 10^{38}–10^{40} ergs. They are observed at high Galactic latitudes and have anomalously high dispersion measure values (e.g., Lorimer et al. 2007; Thornton et al. 2013; Katz 2016). So far, no electromagnetic counterpart has been detected in other frequency bands.

Several models have recently been introduced in the literature to explain the progenitors of FRBs. These models include magnetar flares (Popov & Postnov 2010, p. 129, 2013; Totani 2013; Kulkarni et al. 2014; Lyubarsky 2014), annihilating mini black holes (BHs; Keane et al. 2012), mergers of binary white dwarfs (Kashiyama et al. 2013), the delayed collapse of supermassive neutron stars (NSs) to BHs (Falcke & Rezzolla 2014), flaring stars (Loeb et al. 2014), superconducting cosmic strings (Yu et al. 2014), relevant short gamma-ray bursts (GRBs; Zhang 2014), collisions between NSs and asteroids/comets (Geng & Huang 2015), soft gamma repeaters (Katz 2015), BH batteries (Mingarelli et al. 2015), quark novae (Shand et al. 2016), coherent Bremsstrahlung in strong plasma turbulence (Romero et al. 2016), and young supernova (SN) remnant pulsars (Connor et al. 2016; Cordes & Wasserman 2016). Recently, FRB 140514 was found to be $21 \pm 7\%$ (3σ) circularly polarized on the leading edge with a 1σ upper limit on linear polarization $<10\%$ (Petroff et al. 2015). This provides important constraints on the progenitors. In addition, FRBs may be used as a viable probe to constrain cosmography (e.g., Gao et al. 2014; Zhou et al. 2014). All in all, FRBs are among the most mysterious sources known in current astronomy.

In this paper, we propose that FRBs can arise when a Kerr–Newman BH (KNBH) suddenly discharges. The process destroys the source of the magnetic field associated with the ergospheric motion of the electric field lines. The field then recombines at the speed of light, coherently exciting the ambient plasma and producing a radio pulse. If the KNBH is part of a binary system, then the instability is triggered by tidal interactions in the pre-merging phase. This results in an FRB precursor of the gravitational wave (GW) burst.

The Kerr–Newman (KN) metric has been widely studied since Newman and Janis found the axisymmetric solution of Einstein's field equation for a spinning charged BH (Newman & Janis 1965). In astrophysics, it is generally believed that a KNBH or a Reissner–Nordström BH (RNBH) could not exist for a long time in a plasma environment because the charge accretion would neutralize the BH on short timescales (Ruffini 1973). However, the charge distribution in the magnetosphere can be time stationary when the rotation of the plasma balances the electrostatic attraction of the BH (Punsly 1998). Once mechanical equilibrium is broken because of magnetosphere instability, the electromagnetic energy can be released from the KNBH.

KNBHs have had only limited applications in astrophysics so far: they were invoked to explain some unidentified, low-latitude, gamma-ray sources observed early on by EGRET (e.g., Punsly et al. 2000; Torres et al. 2001, 2003; Eiroa et al. 2002) and gravitational lensing effects (e.g., Kraniotis 2014).

In what follows, we focus on the magnetosphere instability of a KNBH and its possible consequences related to FRBs and their potential afterglows. In Section 2, we describe the initial state of a KNBH, calculate the unstable orbits of a charged test particle surrounding a KNBH, plot the falling trajectories of a test particle, and estimate the corresponding discharge timescale. The radiation mechanism is discussed in Section 3. In Section 4, we briefly mention that the merger of a KNBH binary is one of the plausible central engines of FRBs and their possible afterglows. A short discussion and conclusions are presented in Sections 5 and 6, respectively.

2. MODEL

2.1. Unstable Orbits of a Test Charged Particle

For simplicty, we discuss the unstable orbits of a test charged particle in the magnetosphere. In the geometric unit system ($G = c = 1$), the KN spacetime with mass M, angular momentum J, and electric charge Q can be written in Boyer-Lindquist coordinates as (Misner et al. 1973)

$$ds^2 = -\frac{\Delta}{\rho^2}[dt - a\sin^2\theta d\phi]^2 + \frac{\sin^2\theta}{\rho^2}[(r^2 + a^2)d\phi - adt]^2 + \frac{\rho^2}{\Delta}dr^2 + \rho^2\, d\theta^2, \tag{1}$$

where

$$\Delta = r^2 - 2Mr + a^2 + Q^2, \tag{2}$$

$$\rho^2 = r^2 + a^2\cos^2\theta, \tag{3}$$

and $a = J/M$ is the angular momentum per unit mass. According to $\Delta = 0$, the KNBH horizon can be defined as

$$r_{\rm H} = M + \sqrt{M^2 - a^2 - Q^2}\,. \tag{4}$$

For a KNBH, the mass, spin, and charge should satisfy the relation $M^2 \geqslant a^2 + Q^2$. Furthermore, the angular velocity of the horizon is

$$\Omega_{\rm H} = \frac{a}{r_{\rm H}^2 + a^2}. \tag{5}$$

Here, we just discuss the case of $M > a \gg Q > 0$.

Following the notation of Misner et al. (1973), the electromagnetic vector potential is

$$\boldsymbol{A} = \left(-\frac{Qr}{\rho^2}, 0, 0, \frac{Qra\sin^2\theta}{\rho^2}\right), \tag{6}$$

where bold face indicates the vector. The electromagnetic vector potential $\boldsymbol{A}$ depends on the charge Q and the specific angular momentum a (Hackmann & Xu 2013). The magnetic field is generated by the rotation of the charge distribution and the co-rotation of the charged BH electric field in the ergosphere.

The motions of the neutral test particles in the gravitational field or KN spacetime have been studied in some recent papers (e.g., Liu et al. 2009, 2010, 2011; Pugliese et al. 2013). Let a test particle of rest mass m with charge e be outside a KNBH and let us restrict ourselves to the case of orbits on the equatorial plane $\theta = \pi/2$. The contravariant components of the test particle's four-momentum (namely, Carter's equations, see Carter 1968), $p^\alpha = dx^\alpha/d\lambda$, on the equatorial plane can be expressed as (Misner et al. 1973)

$$p^\theta = 0, \tag{7}$$

$$r^2 p^{\rm r} = \sqrt{R}, \tag{8}$$

$$r^2 p^\phi = -(aE - L_z) + \frac{a}{\Delta}P, \tag{9}$$

$$r^2 p^t = -a(aE - L_z) + \frac{r^2 + a^2}{\Delta}P, \tag{10}$$

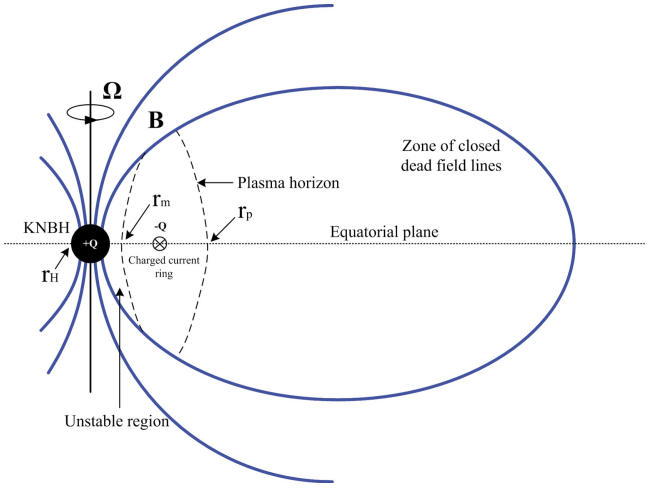

Figure 1. Schematic diagram of the initial state of a KNBH.

and the functions of R and P on the equatorial plane are defined by

$$R = P^2 - \Delta[m^2r^2 + (L_z - aE)^2], \tag{11}$$

$$P = (r^2 + a^2)E - aL_z - eQr, \tag{12}$$

where L_z is the axial component of the angular momentum of the test particle. According to Equations (7)–(10), we can calculate the falling timescale and describe the infalling trajectories of the test particle on the equatorial plane.

From the equation of the radial momentum $p^{\rm r}$, given by Equation (8), the effective potential approach can then be adapted to study the dynamics of the particle. The radial motion is governed by the energy equation

$$E = \frac{\beta}{\alpha} + \frac{\sqrt{\beta^2 - \alpha\gamma_0 + \alpha r^4 (p^{\rm r})^2}}{\alpha}, \tag{13}$$

where α, β, and γ_0 are functions of r and of the constants of motion, written as follows:

$$\alpha = (r^2 + a^2)^2 - a^2\Delta > 0, \tag{14}$$

$$\beta = (L_z a + eQr)(r^2 + a^2) - L_z a\Delta, \tag{15}$$

$$\gamma_0 = (L_z a + eQr)^2 - L_z^2\Delta - m^2r^2\Delta. \tag{16}$$

Qualitative features of the radial motion can be derived from the effective potential $V(r)$, which is given by the minimum allowed value of E at radial coordinate r:

$$V(r) = \frac{\beta}{\alpha} + \frac{\sqrt{\beta^2 - \alpha\gamma_0}}{\alpha}. \tag{17}$$

The circular orbits can be deduced from the equation

$$\frac{dV}{dr} = 0, \tag{18}$$

and the unstable orbit condition is given by

$$\frac{d^2V}{dr^2} < 0. \tag{19}$$

Here, we define $r_{\rm m}$, which is satisfied with $dV/dr = d^2V/dr^2 = 0$, and thus the unstable orbits on the equatorial plane are in the range between $r_{\rm m}$ and the KNBH horizon $r_{\rm H}$, as shown in Figure 1. The units of r are GM/c^2 (or

$r_g/2$). r_m should be larger than the marginally stable circular orbit to ensure that the test particle is out of the horizon. In the following descriptions, we use the normalized units until the BH mass M_{BH} is given in units of $M_\odot$.

2.2. Initial State of a KNBH

The initial steady state configuration of a KNBH is shown in Figure 1. The bulk of the opposite charges of the magnetosphere form an equatorial current ring, which exists in an area wrapped by a plasma horizon, corresponding to the radius with $r_m < r < r_p$ on the equatorial plane. The cause of this is that the quadrupole moment of the electric field dominates at radii larger than that of the ring, while the magnetic field is dipolar. At large enough radius, the particles can exist in $\boldsymbol{E} \times \boldsymbol{B}$ ($\boldsymbol{E}$ and $\boldsymbol{B}$ are the strengthes of the electric and magnetic fields) drift trajectories and are not sucked into the KNBH.

From the plasma equilibrium condition, r_p should meet the following:

$$\left[\frac{\Delta}{(r^2+a^2)^2 - a^2\Delta\sin^2\theta}\right]^{\frac{1}{2}} r^2\rho\sin\theta|_{r=r_p} = \frac{Q}{B}, \qquad (20)$$

which is consistent with the results of RNBHs for $a = 0$ (e.g., Hanni 1975; Damour et al. 1978; Karas & Vokrouhlický 1991). Here, B is the modulus of the magnetic field. If we assume that the ring is located at $r = 10M$, and if $B = 2aQ/r^3$ on the equatorial plane, then r_p is about 23 r_H for $Q \ll a \sim M$. In addition, the closed dead field lines shown in Figure 1 avoid the KNBH from spontaneous electric discharge. This point has been studied in detail in Punsly (1998).

2.3. Results

Figure 2 shows the unstable region on the equatorial plane ($r_H < r < r_m$) around a KNBH ($M = 1$) as a function of the KNBH spin and charge (panel (a)) for $m = 10^{-15}$ and $e = L_z = 10^{-10}$, and the specific charge of the particle (panel (b)) for $a = 0.1$, $Q = 10^{-3}$, and $L_z = 10^{-10}$ (normalized units). From Figure 2(a), we can see that for a test particle, the size of the unstable regions decreases with the increase of the KNBH spin and is almost independent of the KNBH charge up to where its value is close to $\sqrt{M^2 - a^2}$. Figure 2(b) displays the constraint of the unstable regions on the characteristics of the test particle. The unstability conditions require the high-mass particles to have larger values of the charge. In such a case, the specific charge must be less than about 4×10^4 for particles with different masses. According to Figure 2, the resulting unstable orbits reasonably lie in the range 1.5–3.

Since the detected FRBs have variability on millisecond timescales, which indicates that the emission region of the FRBs is very compact, the BH mass can then be restricted to within a few dozen times the solar mass. For a stellar-mass KNBH of $M_{BH} \sim 20\,M_\odot$, the unstable orbit for a charged particle is calculated to be about 10^7–10^8 cm, and the unstable timescale can be estimated to be ~1 ms, which is the typical timescale of FRBs. The charged particles may distribute above or below the equatorial plane of the KNBH, and thus the unstable orbits may be larger than the orbits for the rest particle on the equatorial plane of KNBH, which lead to a falling timescale more in line with the FRB time.

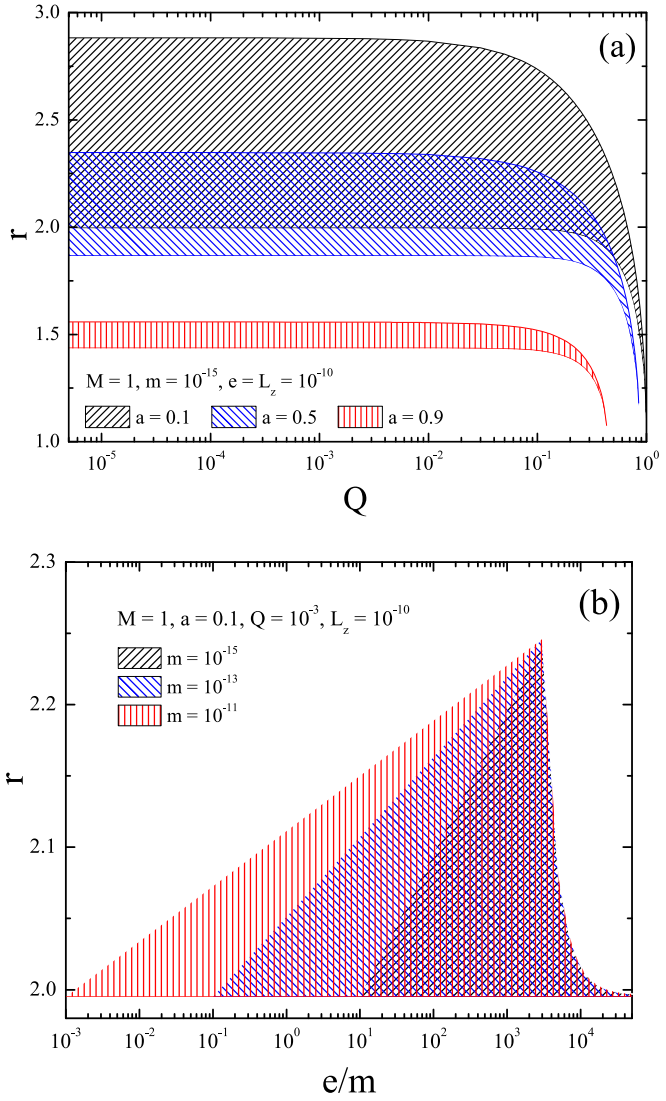

Figure 2. Unstable region on the equatorial plane ($r_H < r < r_m$) around a KNBH ($M = 1$) as a function of the KNBH spin and charge (panel (a)) with $m = 10^{-15}$ and $e = L_z = 10^{-10}$, and the specific charge of the particle (panel (b)) with $a = 0.1$, $Q = 10^{-3}$, and $L_z = 10^{-10}$.

By using Equations (8) and (9), we can plot the falling trajectories of a test particle. Figure 3 shows the trajectories of a test particle ($m = 10^{-15}$, and $e = L_z = 10^{-10}$) on the equatorial plane falling into a KNBH ($M = 1$, $a = 0.1$, and $Q = 10^{-3}$) from $r_0 = 2.5$ to the inner boundary ($r = r_g$) for $E = 1.93 \times 10^{-11}$, 2×10^{-11}, and 2.4×10^{-11}. From Equation (13), the minimum value of E is about 1.92×10^{-11} at $r_0 = 2.5$ in this case. According to Equation (10), the corresponding falling timescales can be calculated as 15.19, 13.28, and 11.26, respectively. For the BH mass $M_{BH} \sim 20\,M_\odot$, the falling timescale is about 1 ms, which coincides with the FRB timescale.

3. RADIATION MECHANISM

The electromagnetic structure of KNBHs is similar to that of NSs in pulsars. However, there are two major differences. First, BHs have no solid surfaces, and consequently there is no thermal emission (Punsly et al. 2000). Second, for KNBHs, the rotation axis and magnetic axis are always aligned. KNBH,

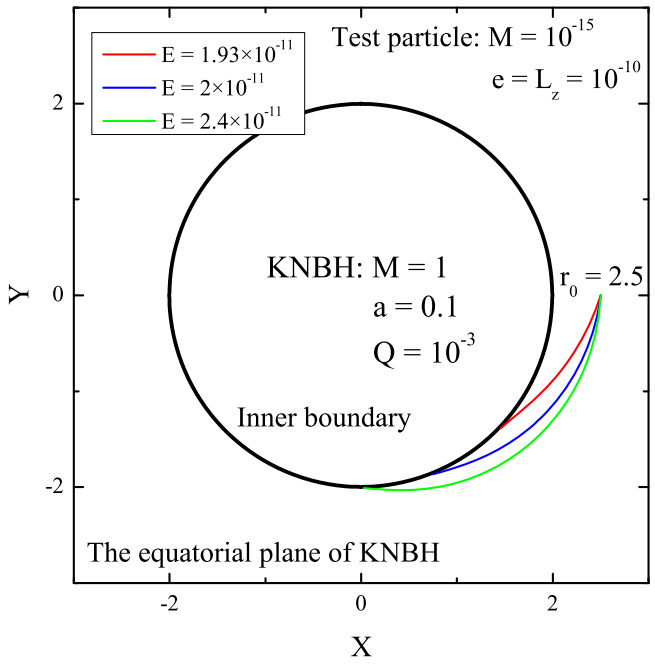

Figure 3. Trajectories of a test particle ($m = 10^{-15}$, and $e = L_z = 10^{-10}$) on the equatorial plane falling into a KNBH ($M = 1$, $a = 0.1$, and $Q = 10^{-3}$) from $r_0 = 2.5$ to the inner boundary ($r = r_g$) for $E = 1.93 \times 10^{-11}$, 2×10^{-11}, and 2.4×10^{-11}.

then, are non-pulsating sources. These features can be used to differentiate them from NSs.

Totani (2013) suggested that binary NS mergers are a possible origin of FRBs, and the radiation mechanism is coherent radio emission, like in radio pulsars. Falcke & Rezzolla (2014) proposed the alternative scenario of a supermassive NS collapsing to a BH. In such a case, the entire magnetic field should in principle detach and reconnect outside the horizon. This results in large currents and intense radiation when the resulting strong magnetic shock wave moves at the speed of light through the remaining plasma. This very same mechanism should operate immediately after the discharge of a KNBH. For a magnetic field strength of $\sim 10^{12}$–10^{13} G the expected energy-loss rate of KNBHs can meet the requirements of FRBs (Falcke & Rezzolla 2014). Also, as in the case of NSs, the radiation from KNBHs can bring the observed polarizations.

If the period of the KNBH is P, which is related to the BH mass and spin, i.e., $P \approx 4\pi G M_{\rm BH}(1 + \sqrt{1 - a_*^2})/a_* c^3$ for $a_* = a/M$ and $a \gg Q$ from Equation (5), the size of its magnetosphere will be

$$R_{\rm mag} = c/\Omega \approx 4.8 \times 10^9 P \ {\rm cm}. \quad (21)$$

For $P = 0.01$ s ($a \approx 0.24$ for BH mass $M_{\rm BH} \sim 20\,M_\odot$), $R_{\rm mag} \sim 5 \times 10^6$ cm and the magnetic shock wave will collectively excite the plasma in $\sim$0.5 ms.

The curvature radiation power emitted per charge is

$$P_e = 2\gamma^4 e^2 c/3R_{\rm mag}^2, \quad (22)$$

and the corresponding frequency is

$$\nu \approx 7\gamma^3 [R/(10^6\ {\rm cm})]^{-1}\ {\rm kHz}. \quad (23)$$

The bulk of the observed radio emission is then generated by particles with $\gamma \sim 1000$. This radiation is well above the relativistic plasma frequency $\nu_{\rm p} = \gamma^{-3/2}(4\pi n_e e^2/m_e)^{1/2} \sim 1$ GHz. The total power of the coherent pulse will be $P_{\rm tot} \sim (n_e V)^2 P_e$, where V is the volume occupied by the plasma of density n_e (for coherent curvature radiation, see Ruderman & Sutherland 1975 and Buschauer & Benford 1976). Typically, $P_{\rm tot} \sim 10^{42}$ erg s^{-1} (e.g., Falcke & Rezzolla 2014).

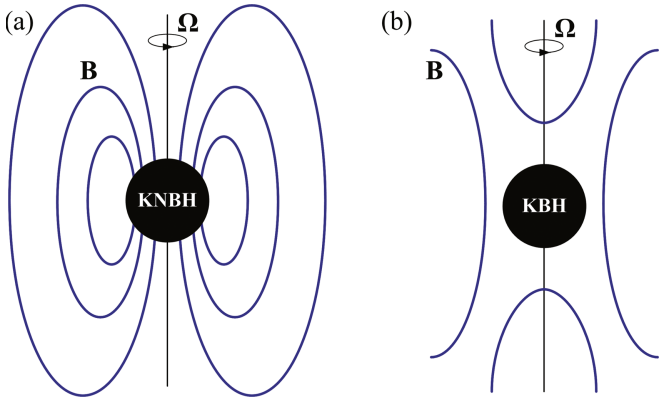

Figure 4. Schematic diagram of the magnetic field configuration during the discharging of a KNBH in a binary.

4. KNBH BINARIES AND FRB AFTERGLOWS

Recently, GW 150914 was detected by the Laser Interferometer Gravitational wave Observatory (LIGO). The GWs originated from the merger of a BH binary. The masses and spins of the two initial BHs are $36^{+5}_{-4}\,M_\odot$, $29^{+4}_{-4}\,M_\odot$ and $<0.69 \pm 0.05$, $<0.88 \pm 0.10$, respectively, and the mass and spin of the BH after merger is $62^{+4}_{-4}\,M_\odot$ and $0.67^{+0.05}_{-0.07}$, respectively (Abbott et al. 2016; Zhang 2016a).

A binary system BH might have a KNBH as one of its components (the younger one). When the holes are close to merging, the tidal forces should perturb the magnetosphere, which would then partially fall into the BH, neutralizing its charge and triggering FRBs through the subsequent magnetic wave. Hence, a FRB might be a signal announcing an imminent GW burst. After the discharge of the BH, the field lines close to the rotation axis will reconnect, sweeping away all of the residual plasma and ejecting a relativistic plasmoid. When such a plasmoid reaches the outer medium, a shock will form. Such a shock can transform part of the kinetic energy of the blob into internal energy in the form of relativistic particles, which might in turn cool through synchrotron and inverse Compton losses producing both radio and gamma-ray emission as in the external shock model of GRBs (e.g., Gao et al. 2013). These two steps are schematically represented in Figures 4(a) and (b), which are similar to Figure 14 in Lehner et al. (2012).

Recently, Punsly & Bini (2016) proposed that the electric discharge of a meta-stable KNBH intermediate state would allow the operation of the magnetic field shedding model of FRBs. In such a model, the collapse of a magnetosphere onto a BH can generate a strong outward Poynting flux (Hanami 1997), which should produce a radio and/or gamma-ray pulse.

In this scenario, the detectability of the FRB afterglow depends on the direction of the BH angular momentum (i.e., the rotation axis or the magnetic axis) and the ejecta opening angle. If the rotation axes of both BHs are almost aligned with

the observer line of sight before the merger, then an FRB and the subsequent afterglow might be detectable.

5. DISCUSSION

We suggest that the magnetospheric instability of a lone KNBH and a KNBH binary may result in FRBs and their afterglows.

In general, there are two possible ways of creating KNBHs. An isolated, uncharged BH may be charged when it strays into the plasma environment, or a charged BH with an oppositely charged magnetosphere may be the direct result of the gravitational collapse of a magnetized star (Punsly 1998). The sudden discharge of these BHs through the instability of their magnetosphere should produce an FRB, but only if the BH spin is pointing nearly toward the observer should a high-energy counterpart be observed. In addition, other mechanisms, such as the implosion of an NS or a jet interaction with a turbulent, low-density plasma, might also generate a similar phenomenon, at least in the radio domain. We consider that the event rate of KNBH-induced FRBs should be only a fraction of the total event rate of FRBs, which is estimated to be around $10^{-3}\,\mathrm{gal}^{-1}\,\mathrm{yr}^{-1}$ (e.g., Thornton et al. 2013; Zhang 2014).

How can we differentiate between the mechanisms proposed here and their competitors? The gravitational signal of colliding BHs in a binary might be a new multi-messenger channel to archive this. The *Fermi* Gamma-ray Burst Monitor recorded a weak gamma-ray transient 0.4 s after GW 150914 (Connaughton et al. 2016). Several models have been proposed to explain the possible electromagnetic counterpart of GW 150914 (e.g., Li et al. 2016; Loeb 2016; Perna et al. 2016; Zhang 2016a). As can be concluded from the above discussion, an alternative not invoking accretion might be related to the presence of a KNBH in the system. In such a case, precursor FRBs might be detectable. The coordination of radio, gamma, and GW observations might result in a tool that is adequate to test the ideas presented here: if an FRB is observed preceding a merger BH and it is followed by a short transient of high-energy radiation, then we might rule out other possibilities such as direct NS collapse and coherent emission excited in ambient plasma by a relativistic jet. In such a situation, the present model should be strongly favored.

6. CONCLUSIONS

We proposed that charged and rotating BHs might be responsible for at least some FRBs when they discharge as a consequence of perturbations in their charged magnetospheres. Our model predicts that if the right ambient conditions are present, then the FRB might be followed by high-energy transients and a longer radio afterglow, similar to GRBs (e.g., Luo et al. 2013; Hou et al. 2014; Liu et al. 2015a, 2015b; Song et al. 2015, 2016). In the case of BH binaries, if one of the holes is a KNBH surrounded by a magnetosphere, then the FRB can be associated with a GW burst, such as that recently detected by the LIGO and VIRGO Collaborations.

We thank Bing Zhang, Brian Punsly, Wei-Min Gu, and Cui-Ying Song for helpful discussions, and the anonymous referee for very useful suggestions and comments. This work is supported by the National Basic Research Program of China (973 Program) under grant 2014CB845800, the National Natural Science Foundation of China under grants 11473022, 11475143, U1331101, and U1431107, and Science and Technology Innovation Talents in Universities of Henan Province under grant 14HASTIT043. G.E.R. is supported by grant AYA 2013-47447-C3-1-P (Spain).

Note Added. Two days after this paper was posted on arXiv, Keane and his collaborators declared that they discovered FRB 150418 and a subsequent fading radio transient lasting ~6 days (Keane et al. 2016). The transient can be used to identify the host galaxy. They concluded that the 6 day transient is largely consistent with a short GRB radio afterglow, but both its existence and timescale do not support progenitor models such as giant pulses from pulsars and SNe. Vedantham et al. (2016) conducted radio and optical follow-up observations of the afterglow, and argued that it may be associated with an AGN, not with FRB 150418, which is also discussed in the literature (e.g., Li & Zhang 2016; Williams & Berger 2016). The isotropic energy of the afterglow is about 10^{50} erg and the beaming-corrected energy is below 10^{49} erg (Zhang 2016b), which can be explained by synchrotron radiation as well as the external shock model in GRBs if the afterglow is associated with FRB 150418. Our model, on the other hand, can explain this event without invoking a GRB or an AGN.

REFERENCES

Abbott, B. P., Abbott, R., Abbott, T. D., et al. 2016, PhRvL, 116, 061102
Buschauer, R., & Benford, G. 1976, MNRAS, 177, 109
Carter, B. 1968, PhRv, 174, 1559
Connaughton, V., Burns, E., Goldstein, A., et al. 2016, arXiv:1602.03920
Connor, L., Sievers, J., & Pen, U.-L. 2016, MNRAS, 458, L19
Cordes, J. M., & Wasserman, I. 2016, MNRAS, 457, 232
Damour, T., Hanni, R. S., Ruffini, R., & Wilson, J. R. 1978, PhRvD, 17, 1518
Eiroa, E. F., Romero, G. E., & Torres, D. F. 2002, PhRvD, 66, 024010
Falcke, H., & Rezzolla, L. 2014, A&A, 562, A137
Gao, H., Lei, W. H., Zou, Y. C., Wu, X. F., & Zhang, B. 2013, NewAR, 57, 141
Gao, H., Li, Z., & Zhang, B. 2014, ApJ, 788, 189
Geng, J. J., & Huang, Y. F. 2015, ApJ, 809, 24
Hackmann, E., & Xu, H. 2013, PhRvD, 87, 124030
Hanami, H. 1997, ApJ, 491, 687
Hanni, R. S. 1975, NYASA, 262, 133
Hou, S.-J., Liu, T., Gu, W.-M., et al. 2014, ApJL, 781, L19
Karas, V., & Vokrouhlický, D. 1991, JPhy1, 1, 1005
Kashiyama, K., Ioka, K., & Mészáros, P. 2013, ApJL, 776, L39
Katz, J. I. 2015, arXiv:1512.04503
Katz, J. I. 2016, ApJ, 818, 19
Keane, E. F., Johnston, S., Bhandari, S., et al. 2016, Natur, 530, 453
Keane, E. F., Stappers, B. W., Kramer, M., & Lyne, A. G. 2012, MNRAS, 425, L71
Kraniotis, G. V. 2014, GReGr, 46, 1818
Kulkarni, S. R., Ofek, E. O., Neill, J. D., Zheng, Z., & Juric, M. 2014, ApJ, 797, 70
Lehner, L., Palenzuela, C., Liebling, S. L., Thompson, C., & Hanna, C. 2012, PhRvD, 86, 104035
Li, X., Zhang, F.-W., Yuan, Q., et al. 2016, arXiv:1602.04460
Li, Y., & Zhang, B. 2016, arXiv:1603.04825
Liu, M., Lu, J., & Gui, Y. 2009, EPJC, 59, 107
Liu, M., Lu, J., Yu, B., & Lu, J. 2011, GReGr, 43, 1401
Liu, M., Yu, B., Yu, F., & Gui, Y. 2010, EPJC, 67, 507
Liu, T., Hou, S.-J., Xue, L., & Gu, W.-M. 2015a, ApJS, 218, 12
Liu, T., Lin, Y.-Q., Hou, S.-J., & Gu, W.-M. 2015b, ApJ, 806, 58
Loeb, A. 2016, ApJL, 819, L21
Loeb, A., Shvartzvald, Y., & Maoz, D. 2014, MNRAS, 439, L46
Lorimer, D. R., Bailes, M., McLaughlin, M. A., Narkevic, D. J., & Crawford, F. 2007, Sci, 318, 777
Luo, Y., Gu, W.-M., Liu, T., & Lu, J.-F. 2013, ApJ, 773, 142
Lyubarsky, Y. 2014, MNRAS, 442, L9
Mingarelli, C. M. F., Levin, J., & Lazio, T. J. W. 2015, ApJL, 814, L20
Misner, C. W., Thorne, K. S., & Wheeler, J. A. 1973, Gravitation (San Francisco: Freeman)

Newman, E., & Janis, A. 1965, JMP, 6, 915
Perna, R., Lazzati, D., & Giacomazzo, B. 2016, ApJL, 821, L18
Petroff, E., Bailes, M., Barr, E. D., et al. 2015, MNRAS, 447, 246
Popov, S. B., & Postnov, K. A. 2010, in Proc. of the Conference dedicated to Viktor Ambartsumian's 100th anniversary Evolution of Cosmic Objects Through their Physical Activity ed. H.A. Harutyunian, A.M. Mickaelian & Y. Terzian (Gitutyun Publishing House of NAS RA)
Popov, S. B., & Postnov, K. A. 2013, arXiv:1307.4924
Pugliese, D., Quevedo, H., & Ruffini, R. 2013, PhRvD, 88, 024042
Punsly, B. 1998, ApJ, 498, 640
Punsly, B., & Bini, D. 2016, MNRAS, 459, L41
Punsly, B., Romero, G. E., Torres, D. F., & Combi, J. A. 2000, A&A, 364, 552
Romero, G. E., del Valle, M. V., & Vieyro, F. L. 2016, PhRvD, 93, 023001
Ruderman, M. A., & Sutherland, P. G. 1975, ApJ, 196, 51
Ruffini, R. 1973, in Black Holes, ed. B. Dewitt & C. Dewitt (New York: Gordon & Breach), 525
Shand, Z., Ouyed, A., Koning, N., & Ouyed, R. 2016, RAA, 16, 80
Song, C.-Y., Liu, T., Gu, W.-M., et al. 2015, ApJ, 815, 54
Song, C.-Y., Liu, T., Gu, W.-M., & Tian, J.-X. 2016, MNRAS, 458, 1921
Thornton, D., Stappers, B., Bailes, M., et al. 2013, Sci, 341, 53
Torres, D. F., Romero, G. E., Combi, J. A., et al. 2001, A&A, 370, 468
Torres, D. F., Romero, G. E., Eiroa, E. F., Wambsganss, J., & Pessah, M. E. 2003, MNRAS, 339, 335
Totani, T. 2013, PASJ, 65, 12
Vedantham, H. K., Ravi, V., Mooley, K., et al. 2016, ApJL, 824, L9
Williams, P. K. G., & Berger, E. 2016, ApJL, 812, L22
Yu, Y.-W., Cheng, K.-S., Shiu, G., & Tye, H. 2014, JCAP, 11, 040
Zhang, B. 2014, ApJL, 780, L21
Zhang, B. 2016a, arXiv:1602.04542
Zhang, B. 2016b, ApJL, 822, L14
Zhou, B., Li, X., Wang, T., Fan, Y.-Z., & Wei, D.-M. 2014, PhRvD, 89, 107303